

Hierarchical Windowed Graph Attention Network and a Large Scale Dataset for Isolated Indian Sign Language Recognition

Suvajit Patra
RKMVERI
Belur, India

suvajit.patra.cs20@gm.rkmvu.ac.in

Arkadip Maitra
RKMVERI
Belur, India

arkadipmaitra@gmail.com

Megha Tiwari
FDMSE, RKMVERI
Coimbatore, India

mghgpt84@gmail.com

K. Kumaran
FDMSE, RKMVERI
Coimbatore, India

k6kumaran@gmail.com

Swathy Prabhu
RKMVC
Chennai, India

swathyprabhu@gmail.com

Swami Punyeshwarananda
RKMVERI
Belur, India

punyeshwarananda@gm.rkmvu.ac.in

Soumitra Samanta
RKMVERI
Belur, India

soumitra.samanta@gm.rkmvu.ac.in

Abstract

Automatic Sign Language (SL) recognition is an important task in the computer vision community. To build a robust SL recognition system, we need a considerable amount of data which is lacking particularly in Indian sign language (ISL). In this paper, we introduce a large-scale isolated ISL dataset and a novel SL recognition model based on skeleton graph structure. The dataset covers 2002 daily used common words in the deaf community recorded by 20 (10 male and 10 female) deaf adult signers (contains 40033 videos). We propose a SL recognition model namely Hierarchical Windowed Graph Attention Network (HWGAT) by utilizing the human upper body skeleton graph. The HWGAT tries to capture distinctive motions by giving attention to different body parts induced by the human skeleton graph. The utility of the proposed dataset and the usefulness of our model are evaluated through extensive experiments. We pre-trained the proposed model on the presented dataset and fine-tuned it across different sign language datasets further boosting the performance of 1.10, 0.46, 0.78, and 6.84 percentage points on INCLUDE [44], LSA64 [39], AUTSL [43] and WLASL [22] respectively compared to the existing state-of-the-art keypoints-based models. The proposed dataset and the model implementation code will be available at <https://cs.rkmvu.ac.in/~isl>.

1. Introduction

Sign Language (SL) is a natural language with unique grammatical and linguistic characteristics. The deaf and mute community developed this to socialize and communicate with each other. As a visual language, SL conveys information by articulation of human body parts with manual characteristics such as hand shapes, body pose, and the interaction of hands with different body parts, together with non-manual characteristics such as facial expression and head movement [1, 40].

According to the World Health Organization (WHO), around 5% (430 million) of people around the world suffer from hearing loss [10]. To bridge the communication gap between signers (people with sign language as their primary communication medium) and non-signers (people with spoken language proficiency rather than sign language) the automatic SL recognition field has emerged and gained popularity among computer vision and machine learning researchers [23, 46, 53]. This task contains two subtasks, 1) *isolated SL* recognition - which maps every sign video to the corresponding gloss¹, and 2) *continuous SL* recognition - which maps every sign video to a sequence of glosses. Here our focus is on isolated SL recognition. Similar to any recognition task, building a good SL recognition model, requires an adequate amount of training data so as to get a reasonably accurate inference. Researchers have presented dif-

¹Glosses are distinct units of written form of sign language.

ferent datasets for different sign languages across the world. For instance, MS-ASL [47], WLASL [22], ASLLVD [4] are the datasets for isolated American SL. BOB-SL [3], and BSLDict [29] datasets are for the British SL. Furthermore, there are datasets [39, 43, 53] for other sign languages as well.

The Indo-Pakistani sign language is the most widely used sign language in the world and about 15 million deaf signers use this in their daily communications². In comparison with other sign languages, Indian Sign Language (ISL) contains a higher number of composite signs (signs made up of two or more glosses). For example, the sign for *Wife* consists of the *Female* and *Marriage* signs [44]. This makes the ISL unique and the recognition task challenging. For automatic ISL recognition task, there are not many publicly available resource-rich datasets in the literature. Some limited attempts have been made with INCLUDE [44] and CISLR [17] containing a limited number of sign videos per word. This motivated us to create a large-scale isolated resource-rich ISL dataset, which is called FDMSE-ISL.

The task of sign language recognition is a subdomain of human action recognition from video data and it inherits all the challenges such as motion blur, occlusion of body parts, human appearance, recording environments and fuzzy boundaries between classes [32]. In addition to these, sign language glosses contain very subtle spatial and temporal differentiable features, which introduces another level of complexity. This makes the sign language (particularly ISL) recognition task more challenging than action recognition. Even state-of-the-art action recognition models are inadequate in SL recognition tasks.

To model the SL recognition task we calculate a set of signer’s skeleton joint points from sign videos and represent the point set as a spatio-temporal graph. We model the graph-learning task by adapting an existing popular mechanism used in Natural Language Processing (NLP). Specifically, we make use of the attention mechanism [48] to learn the spatio-temporal graph. In current NLP models, spoken language is represented by a 1-dimensional sequence of words with well-defined syntax and semantics and its structure is successfully modelled by an attention mechanism [48]. However, the keypoint graph extracted from sign videos is 3-dimensional data with complex spatio-temporal context, and it is non-trivial to analogously define a visual word or unit with clarified semantics. The spatio-temporal keypoint data poses difficulty in sign recognition using the existing graph-based and normal baseline approaches. We propose a novel Hierarchical Windowed Graph Attention Network (HWGAT) that redefines the approach to graph input processing. The model introduces constraints on the attention mechanism by utilizing a keypoint graph, combined with a partitioning strategy for the input. Through extensive

experiments, we justify the various design decisions in the HWGAT model. We evaluate the proposed HWGAT model on the presented dataset as well as some other popular SL datasets and draw performance comparisons. In this paper, our main contributions are as follows:

1. We present a large scale isolated ISL dataset FDMSE-ISL consisting of over 40000 videos containing a rich and large vocabulary of 2002 daily used signs in ISL conversations. Some of the unique characteristics are 20 signers, gender-balanced and signer-independent sets (no intersection of signers in training, validation, and testing sets). It also contains sign word analysis and their categorizations into atomic and composite based on the count of glosses per sign.
2. We propose a novel attention-based graph neural network specifically developed for sign language recognition on keypoint graphs.
3. We publish our automated recording and annotations pipeline to ease such data collection process in any sign language.

The rest of the paper is organized as follows: Section 2 provides an overview of the existing sign language datasets and recognition techniques. The characteristics of the presented dataset are described in Section 3. Section 4 presents the working mechanism of the proposed model. The experiments, analysis and results are discussed in Section 5 followed by conclusion in Section 6.

2. Related Works

This section reviews the existing ISL datasets followed by a survey of large scale isolated datasets for other sign languages. We then review some state-of-the-art sign language recognition models from the literature.

For ISL recognition, the initial datasets primarily consists of either a few image samples or less number of sign videos. To the best of our knowledge, the first ISL dataset presented by Rekha *et al.*, consists of 290 images for 26 alphabets [37]. In [30], authors introduced a dataset containing 600 videos corresponding to 22 sign word classes and in [19], the authors present a dataset with 800 sign videos for 80 signs. All these datasets suffer from either a small vocabulary size or a small sample size per class. These datasets are as such inadequate to build models for real-world applications. The largest available ISL dataset CISLR contains 7050 videos with over 4765 sign words [17]. It however suffers from very low per-class samples, making it unusable for real-world sign language recognition tasks, although applicable for one-shot learning tasks. The more recent isolated ISL dataset INCLUDE [44] has a collection of 263 signs, recorded with 7 signers (students) in

²<https://www.ethnologue.com/>

Table 1. Comparison of FDMSE-ISL dataset with existing isolated sign language datasets.

Dataset	Language	# Signs	# Sign video (avg. per sign)	# Signers	Source	# Hours
ASLLVD [4]	American (ASL)	2,742	9K (3)	6	lab	4
ASL-LEX 2.0 [41]	American (ASL)	2,723	2723(1)	-	lexicons, lab, web	-
MSASL [47]	American (ASL)	1,000	25K(25)	222	lexicons, web	25
WLASL [22]	American (ASL)	2,000	21K (11)	119	lexicons, web	14
LSA64 [39]	Argentinian	64	3K (47)	10	-	1.9
BSLDict [29]	British (BSL)	9,283	14K (1)	148	lexicons	9
DEVISIGN-L [49]	Chinese (CSL)	2,000	24K (12)	8	lab	13-33
SLR500 [53]	Chinese (CSL)	500	125K (250)	50	lab	69-139
GSL [1]	Greek (GSL)	310	40K()	7	-	6.4
SMILE [11]	Swiss German (DSGS)	100	9K (90)	30	lab	-
BosphorusSion22k [31]	Turkish (TSL)	744	23K (30)	6	lab	19
AUTSL [43]	Turkish (TSL)	226	38K (170)	43	lab	21
INCLUDE [44]	Indian (ISL)	263	4K (16)	7	lab	3
CISLR [17]	Indian (ISL)	4765	7K (1)	71	web	3
FDMSE-ISL	Indian (ISL)	2,002	40K (20)	20	lab	36

a classroom setting with a static background, and contains a total of 4,287 videos. This dataset too contains limited vocabulary compared to the size of vocabulary used by ISL signers in their daily conversation.

For other sign languages, there exists a number of large scale sign language datasets as shown in Table 1. Athitsos *et al.* [4] proposed an isolated American Sign Language (ASL) dataset called ASLLVD, consisting of 9800 video samples of 3300 sign words, recorded with 1-6 native signers. Another isolated ASL dataset called MS-ASL [47] proposed by Jose and Koller contains 25000 videos of 1000 sign words with 222 signers. To make the dataset generic to ASL they recorded the videos in unconstrained real-life conditions. In the recent past, Li *et al.* [22] proposed a word-level ASL dataset (WLASL) with a total of 21083 video samples of 2000 signs with 119 signers. These videos were collected from various web sources. Momeni *et al.* [29] proposed a British Sign Language (BSL) dataset known as BSLDict which contains a large vocabulary of size 9283 and is created with 148 signers. A dataset for Turkish Sign Language (TSL) published by Sincan and Keles [43] called AUTSL contains 38336 video samples of 226 signs performed by 43 different signers. These videos were recorded in both indoor and outdoor environments. This dataset has color, depth, and skeleton modalities. SLR500 [53] is an isolated Chinese Sign Language (CSL) dataset containing 125000 videos spanning over 500 signs. The SMILE [11] dataset is an isolated Swiss German Sign Language (DSGS) dataset containing 100 signs with 9000 videos.

To the best of our knowledge, in terms of video count, the dataset presented in this paper contains the highest number of videos compared to the other isolated sign language datasets shown in Table 1, with the singular exception of

SLR500 dataset. However, the SLR500 dataset has a small vocabulary of 500 signs only, where each sign is repeated five times by the same signer. Regarding vocabulary size, the sign language dictionaries ASLLVD [4], ASL-LEX 2.0 [41], WLASL [22], and BSLDict [29] have demonstrated either comparable or greater coverage of signs. However, they have fewer videos per sign as shown in Table 1.

In general, researchers try to address the SL recognition task as a pattern recognition task. It contains two subtasks, namely, 1) *feature extraction*: each sign video is represented as a fixed dimensional feature vector, and 2) *recognition*: the represented videos are classified using a standard classifier. For feature extraction, researchers [16, 23, 31, 46, 53] have tried some hand-crafted feature descriptors such as Histogram of Oriented Gradient (HOG) [8], Scale Invariant Feature Transform (SIFT) [25], Optical Flow [13], etc.. They classify each sign using standard classifiers like HMM [21, 33], SVM [35], and Random Forest [2].

In recent years, researchers are employing deep learning-based methods for automatic feature extraction and classification tasks. Specifically, in the domain of SL recognition, deep learning-based methods can be broadly classified into two types. The first approach involves extracting features from each raw RGB video using various methods such as two-dimensional (2D) Convolutional Neural Network (CNN) [20, 36], 3D CNN [14, 22], and CNN models with Bidirectional Long Short Term Memory (Bi-LSTM) decoder [9]. These features are classified into glosses using one or more fully connected layers. In addition to RGB videos, Jiang *et al.* [16] used depth, skeleton, and motion information to improve the recognition of Turkish sign language. Zuo *et al.* [55] further enhanced the performance by

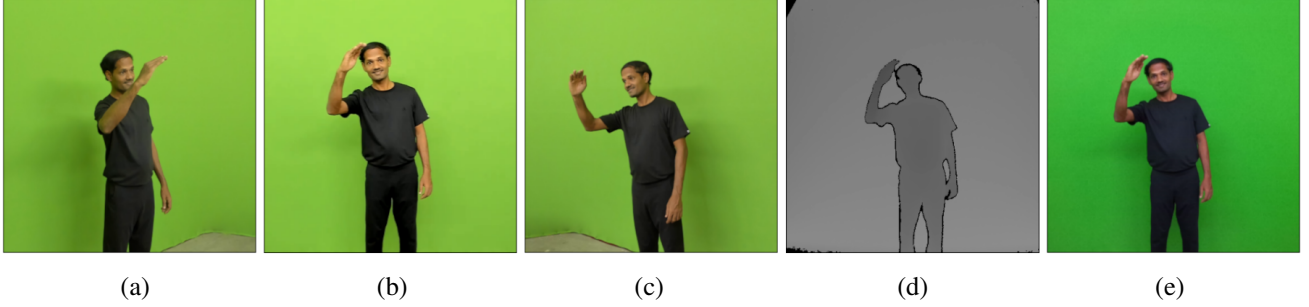


Figure 1. A sample frame of the sign *Hello* in all the views and modalities ((a) left (60fps), (b) front (60fps), (c) right (60fps), (d) Azure Kinect DK depth (30fps) and (e) Azure Kinect DK RGB (30fps)) available in the dataset.

integrating natural language glosses during the training process. Despite these achievements, RGB-based methods are computationally expensive and their slow execution poses limitations for real-time SL recognition.

The second approach typically consists of detecting the keypoints of the signer using the state-of-the-art human pose estimation methods like MediaPipe [26], OpenPose [7], MMPose [28], Yolo-pose [27], HR-Net [50] and others [34, 38, 54]. The extracted sequential pose data is processed using various sequential data models including GRU [22], LSTM [18, 23], and several variants of Transformers [5, 6, 42] for SL recognition task. Further, the sequential pose data is represented as keypoint graphs and input to the Graph Convolutional Networks (GCNs) due to their proven ability to effectively capture contextual information from graphical data. Yan *et al.* [51] first introduced a GCN on the sequential human keypoints data as a spatio-temporal graph using natural human joint connectivity and called it ST-GCN. Jiang *et al.* adopted this model for Turkish sign language recognition, by cascading spatial, temporal and adaptive channel information to the GCN block and called it SL-GCN [16]. The ST-GCN and SL-GCN models were applied to the Indian sign language recognition task on the INCLUDE [42] dataset. During inference, these models perform convolution using fixed kernel weights irrespective of the values of node features.

In this paper, we propose a graph attention-based network named Hierarchical Windowed Graph Attention Network (HWGAT), in which we use an attention mechanism that takes the node features into consideration to generate dynamic attention weights instead of using fixed kernel weights. The method yields promising results compared to other keypoint-based models across several SL datasets.

3. FDMSE-ISL Dataset

In the creation of this dataset, we followed the FDMSE’s [15] ISL dictionary that was published in consultation with sign experts throughout India. We picked 2002

common words from the dictionary that are used in daily communications within the deaf community. In the dictionary these words are categorised into 57 groups such as ‘family relations’, ‘behaviour norms’, ‘body parts’, ‘household articles’ etc. We regrouped them into two classes, namely, atomic signs or glosses (that cannot be decomposed into other meaningful signs (eg., *Marriage*)) and composite signs (can be decomposed into atomic signs or glosses (eg., *Wife* → *Female* + *Marriage*)).

We prepared the dataset with the help of 20 native ISL signers (deaf) from the southern part of India. To ensure that the dataset is gender unbiased, we considered 10 male and 10 female subjects. For data collection setup, we used a static background with a green screen to facilitate image segmentation.

We recorded the videos from four different viewing positions: two *frontal*, 30° *left* and 30° *right* with respect to the *frontal* view of the subject. Three *Logitech BRIO* 60 fps cameras were used for recording the videos in landscape mode with a frame size of 1920 × 1080. Furthermore, to capture the depth information one *Azure Kinect DK* camera was used at the front position. Keeping the single-view real-world SL recognition applications in mind, this work only focuses on the *frontal* RGB camera data. However, all the five recordings (4 RGB and 1 depth modalities) will be made publicly available (<https://cs.rkmvu.ac.in/~isl>) with permission to use for research purposes only. Besides the *frontal* RGB modality, the other multiview data can be used for tasks such as keypoints correction, pose estimation, 3D-model generation, and general gesture recognition. The videos were recorded in the lab settings with requisite ethical clearance and a standard signer dress code (matt black) under the supervision of certified ISL experts.

To simplify the dataset collection process we built a custom tool named ‘Word Viewer and Timeline Manager’ (WVTM) that manages and automatically annotates the entire corpus of videos. While recording, the operator uses the WVTM tool to first show a sign word to the subject with

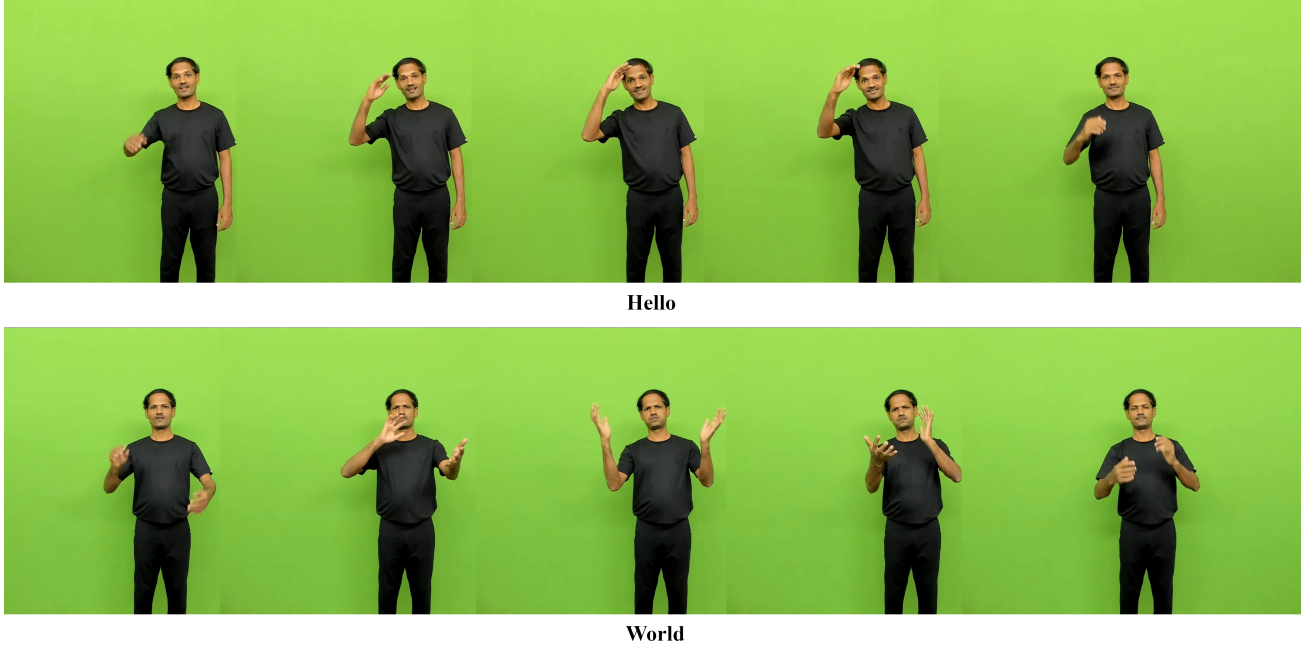


Figure 2. Sample frames from the signs *Hello* and *World*.

a prompt and then to register the event timestamps (session start, start recording for a word, stop recording for a word, session end etc.) in a log file. After recording all the sessions, a Python script is run to automatically split the videos and annotate them using the log files generated during the recording. The complete annotation and recording pipeline will be made public (<https://cs.rkmvu.ac.in/~isl>) to assist users with similar needs.

On the whole, the dataset from the *frontal* RGB camera contains 40033 videos for 2002 words. The total duration of the dataset is around 36.2 hours with 7.8 Million frames. The average duration of the sign videos is around 3.25 seconds. We crop the original videos to 1200×950 resolution keeping the signer at the centre. Table 2 summarizes the statistics of this dataset. For each sign word, there are *five* different modalities (*frontal* both 60 fps and 30 fps, two side views at $\approx \pm 30$ degrees 60 fps and depth information) from *four* viewing positions. *Azure Kinect DK* captured both depth and RGB information at 30 fps. The work presented in this paper uses only the *frontal* 60 fps RGB camera recorded videos. We call this the ‘working dataset’. Fig. 1 shows the sample frames from each camera view and Fig. 2 shows sample frames of two sign words: *Hello* and *World*.

The FDMSE-ISL dataset is richer in several aspects than the well-known ISL dataset INCLUDE [44]. For instance, the presented dataset contains about 7.6 times higher number of signs and 9.3 times higher number of videos. Furthermore, the FDMSE-ISL dataset has more qualitative di-

Table 2. Key features of the FDMSE-ISL dataset.

Characteristics	Values
# words	2002
# videos	40033
# word categories	57
Average videos per class	≈ 20
Average video duration	3.25s
Minimum video duration	1.5s
Maximum Video duration	9.5s
Frame rate	60 fps, 30 fps
Resolution	1200×950 , 512×512
Modalities	4 <i>RGB</i> , 1 <i>depth</i>

versity in terms of age, height, and skin tone. For instance, the INCLUDE [44] dataset was recorded with young students of similar age, whereas the signers’ approximate age ranges between 28 and 55, and height between 4.5 and 6 feet. While the dataset is multimodal and multicamera, the INCLUDE dataset was recorded with a single camera.

To evaluate the proposed model HWGAT on the working dataset, we divide the dataset into train, validation, and test partitions in the ratio 5 : 1 : 4 on randomly chosen subjects (signers) so that the training set, validation set and test set have no common signers across these sets. In total, there are 10 subjects in training (5 male, 5 female), 2 in validation (1 male, 1 female) and 8 in testing (4 male, 4 female). Finally, we used 20016, 4003, and 16014 videos for training, validation, and testing respectively.

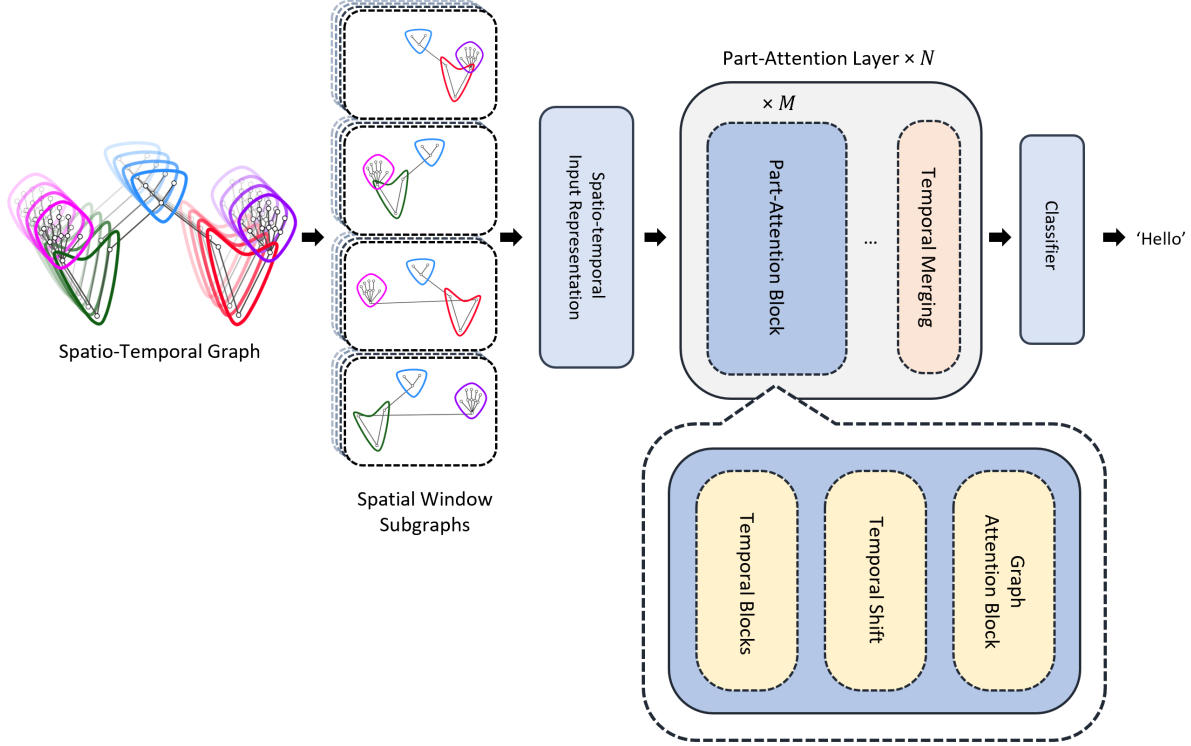


Figure 3. The proposed Hierarchical Windowed Graph Attention Network (HWGAT) takes the spatio-temporal graph structure as input and divides this graph into multiple spatial windows based on distinct body parts as represented in Figure 4. Next, multiple part attention layers are applied on this windowed graph structure to extract features and a fully connected layer is used to get the sign word.

4. Proposed Approach

The objective of this work is to create a sign language recognition system that works on the extracted keypoints from any sign video. The body keypoints and the edges connecting them form a graph, which is further input to a Graph Convolution Network (GCN) [16, 51] for classification. In general, GCN models are similar to CNNs where the learned adjacency matrix in GCN is similar to the kernel in CNN. But, after the training process, the elements of the adjacency matrix are static. We propose a Hierarchical Windowed Graph Attention Network (HWGAT) in which we use an attention mechanism that takes the node features into consideration to generate dynamic attention weights instead of fixed kernel weights, thereby giving importance to the neighbourhood nodes based on their similarity during information propagation. In order to incorporate the importance of body parts for any sign word recognition our attention mechanism is designed to be restricted to the spatio-temporal graph. An overview of the proposed HWGAT is presented in Fig. 3. This model incorporates a spatio-temporal windowed graph as *input representation* and *part-attention layer*. We describe these two components of this model in the following sections:

4.1. Input Representation

The input representation comprises two parts: *spatio-temporal graph* and *spatial window subgraphs*. We select 27 keypoints from each frame of a sign video, that includes 3 facial keypoints (nose, 2 eyes), 2 shoulders, 2 elbows, and 10 keypoints from each hand to represent the spatial graph, shown in Fig. 5. Each keypoint is represented as a 2D vector of x and y coordinates. These keypoints are selected based on recommendations from SL experts and the connection between the keypoints is inspired by Jiang *et al.* [16] and Selvaraj *et al.* [42]. An entire video consisting of F frames gives F distinct spatial graphs and each of these graphs contains $K = 27$ keypoints. These spatial graphs are further interconnected on temporal basis to give the spatio-temporal graph denoted by G . The edge set $E(G)$ is defined as follows:

$$E(G) = \begin{cases} e_{i,j}^t = 1, & \text{if } v_i, v_j \text{ are connected spatially} \\ e_i^{t,t+1} = 1, & \text{temporal connection} \\ e_i^t = 0, & \text{otherwise} \end{cases} \quad (1)$$

where, $t \in \{1, 2, \dots, (F - 1)\}$ denotes the frame index and v_i ($1 \leq i \leq K = 27$) represent a node in the graph.

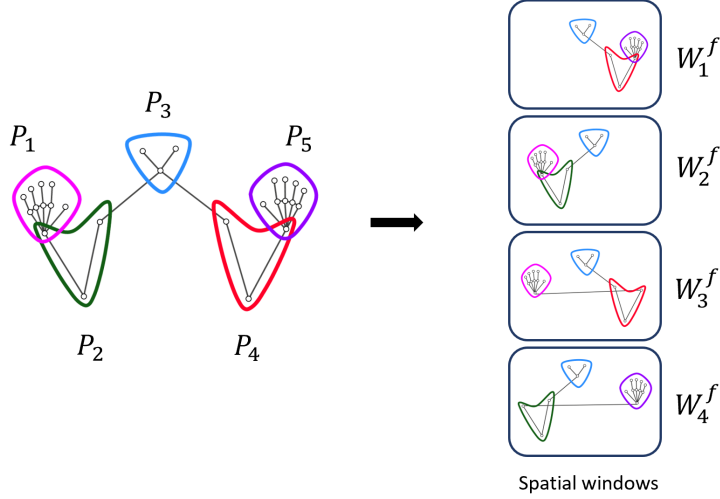


Figure 4. Grouping of keypoints according to the 5 body parts P_1 to P_5 . P_1 contains the right-hand keypoints, P_2 contains the right arm keypoints, P_3 contains the facial keypoints, P_4 corresponds to the left arm and P_5 that of the left hand keypoints. The part combinations are used to create the 4 spatial windows.



Figure 5. Visual representation of the spatial graph using 27 keypoints (10 per hand and 7 pose points).

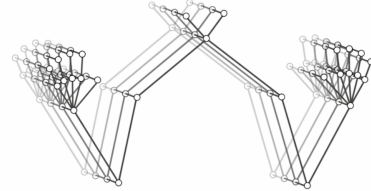


Figure 6. An example of a spatio-temporal graph generated by connecting the nodes of four sequential spatial keypoint graphs through temporal edges.

The Fig. 6 depicts the spatio-temporal graph for four continuous frames in a sign video. Henceforth, the terms node and keypoint are used interchangeably.

A distinctive feature of our model, in contrast to GCNs, is the partitioning of the keypoint graph into spatial windows rather than treating the entire graph as input. In the single-view pose estimation methods, inconsistencies in keypoint generation are inevitable, especially for the hand keypoints. These inconsistencies often arise from factors such as motion blur, occlusion by body parts, and low video resolution. To mitigate these inconsistencies, we divide the keypoint graph into multiple subgraphs called spatial windows. We define 5 subsets for each frame, labeled P_1 to P_5 , for the keypoint set corresponding to body parts:

right hand, right arm, face, left arm, and left hand as illustrated in the Fig. 4. For a frame f we now construct 4 different spatial windows W_j^f , $1 \leq j \leq 4$ in the following manner: $W_1^f = \{P_3, P_4, P_5\}$, $W_2^f = \{P_3, P_2, P_1\}$, $W_3^f = \{P_3, P_4, P_1\}$, $W_4^f = \{P_3, P_2, P_5\}$. It's easy to see that each of the spatial windows W_j^f contain 16 keypoints with two repeated keypoints. The set of 4 spatial windows constructed thus contains a total of $K' = 64$ keypoints. The sign video containing F frames, K keypoints per frame, and dimension $d = 2$ can be seen as an input in the $\mathbb{R}^{F \times K \times d}$ space. The spatial window representation mechanism projects the given input into a new space $\mathbb{R}^{F \times K' \times d}$. The above construction restricts the flow of in-

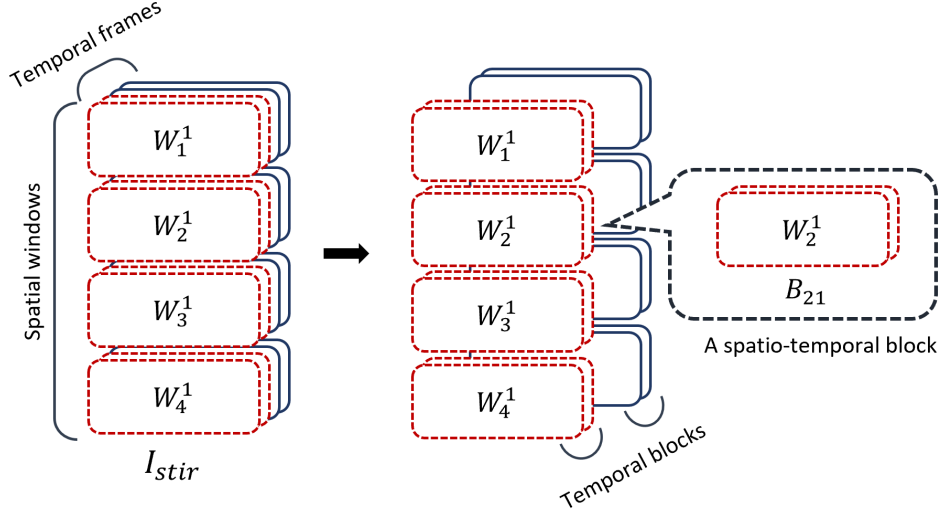


Figure 7. The frames are partitioned into temporal blocks where each temporal block contains two frames. Each spatial window with its respective temporal block forms a spatio-temporal block.

formation from one window to another. As a result, we can see that for single-handed signs the spatial window contains keypoints only of that hand, thereby eliminating the potential interference of the non-signing hand’s motion.

It was demonstrated that the Fourier feature mapping allows a model to learn high-frequency functions more effectively [45]. This mapping involves embedding the low-dimensional input coordinates into a higher-dimensional space. Specifically, our low d dimensional node input representation is embedded into a higher dimension d' using the Fourier feature mapping resulting in the spatio-temporal input representation $I_{stir} \in \mathbb{R}^{F \times K' \times d'}$.

We incorporated the frame position as a sequence marker into the input embeddings using a fixed positional encoding scheme similar to the one proposed by Vaswani *et al.* [48].

4.2. Part Attention Layer

The individual signs are defined by the motion of different parts. In order to learn the motion, the model needs to learn the attention between body parts, for which we design a part-attention layer consisting of *two* key components: *part-attention block*, and *temporal merge* shown in Fig. 3.

4.2.1 Part Attention Block

The part-attention layer is built by cascading multiple part-attention blocks. The various contextual features are accumulated at the nodes through information propagation across the multiple part-attention blocks within each part-attention layer. The part-attention block has *three* key

components, namely, *temporal blocks*, *temporal shift*, and *graph-attention block* shown in Fig. 3.

Temporal Blocks: Temporally consecutive frames tend to have very subtle changes between the spatial graphs. Therefore two successive frames in the spatio-temporal input representation are grouped to form a temporal block for further processing. The formation of temporal blocks aids in applying the hierarchical divide-and-conquer procedure. The attention mechanism is applied within these blocks to capture the local context. Subsequently, these blocks are merged hierarchically upward to capture the entire temporal context. To implement this, the embedded spatio-temporal input representation I_{stir} is partitioned into multiple temporal blocks, each consisting of $T = 2$ successive frames. Let $B_{ij} \in \mathbb{R}^{T \times K' \times d'}$ be the spatio-temporal block which represents the i^{th} spatial window and j^{th} temporal block shown in Fig. 7.

Temporal Shift: In the proposed model, the benefit of restriction of attention within each spatio-temporal block however limits the extent of information propagation between consecutive temporal blocks which is undesirable. To address this issue, we apply a shifting mechanism inspired by Liu *et al.* [24] that shifts by one position in forming the temporal blocks from the input sequence. This aids in propagating information between consecutive temporal blocks.

Graph Attention Block: The graph-attention block, illustrated in Fig. 8, is designed to operate on the spatio-

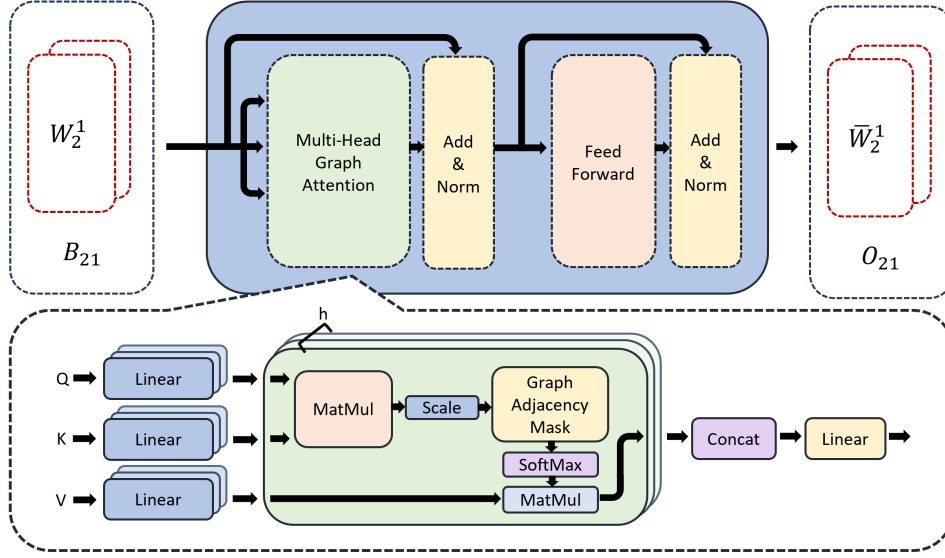


Figure 8. The graph-attention block consists of the multi-head graph attention module along with normalization and feed-forward layers. The multi-head graph attention module utilizes the graph adjacency mask to restrict the attention mechanism.

temporal blocks B_{ij} . This block accumulates information from the neighboring nodes using the attention mechanism that utilizes node feature similarity rather than a convolution kernel. To obey the human joint-bone connectivity the attention mechanism needs to be restricted to the neighboring nodes connected by edges in the spatio-temporal graph. For this, we use an attention mask called *edge bias* following the adjacency in the spatio-temporal graph. The *edge bias* works as the inductive bias in the model. For every spatio-temporal block B_{ij} for i^{th} spatial window and j^{th} temporal block, the attention mask (graph adjacency mask) A_{ij} is constructed using the block’s graph adjacency matrix.

Let n be the total number of keypoints within the $(i, j)^{th}$ spatio-temporal block. Then $B_{ij} \in \mathbb{R}^{n \times d'}$ such that $n = T \times 16$ (each spatial window contains 16 keypoints). We define graph attention ($Attn_G$) and other modules shown in Fig. 8 as follows:

$$\begin{aligned}
 Attn_G &= Softmax\left(\frac{Q \times K^T}{\sqrt{h}} \odot A_{ij}\right) \\
 Q &= Norm(B_{ij}) \times W^q \\
 K &= Norm(B_{ij}) \times W^k \\
 V &= Norm(B_{ij}) \times W^v \\
 B'_{ij} &= B_{ij} + GAttn \times V \\
 O_{ij} &= B'_{ij} + FF(Norm(B'_{ij}))
 \end{aligned} \tag{2}$$

where W^q, W^k, W^v are the model parameters and h is the number of heads, similar to the multi head attention de-

scribed by Vaswani *et al.* [48]. Notations \odot and \times represent the element-wise multiplication and matrix multiplication, respectively. Here we use *layer normalization* as $Norm$ to normalize the input, FF is a feed-forward layer, and the output O_{ij} represents the embedding of B_{ij} which captures the local spatio-temporal contextual information.

We observed that the attention values generated by similar adjacent nodes are high due to their feature similarity (eg. nose keypoints in a temporal block). The high cosine similarity values among these nodes can sometimes reduce the attention values between other nodes, leading to a loss of important information. To overcome this issue, we propose an attention dropout mechanism inspired by Lin *et al.* [52]. However, instead of randomly nullifying attention value, our proposed regularization technique is more likely to drop attention between two nodes with higher attention value. First a random variable γ is uniformly sampled from $(0, 1)$. Then the attention matrix $Attn_G$ is masked with value 0 where $Attn_G$ is greater than γ .

4.2.2 Temporal Merge

This block is the second component of the part-attention layer. Note that the attention mechanism in the first part-attention layer captures the local context. To capture the global context, we use a hierarchical merging technique. In each part-attention layer, following the M graph attention operations (shown in Fig. 3), the number of frames is reduced by merging the frames within each temporal block, resulting in upper-level contextual attention in

the deeper part-attention layer. For a spatio-temporal input $I_{stir} \in \mathbb{R}^{F \times K' \times d'}$ and temporal block size $T = 2$, after first merge (concatenate) we get a spatio-temporal contextual embedding in $\mathbb{R}^{(F/T) \times K' \times (d' \times T)}$.

After N part-attention layers processing, we use an average pooling over all the spatial windows to represent the final spatio-temporal contextual feature embedding. We use a fully connected layer that utilizes this embedded feature to classify each sign.

5. Experimental Evaluation

This section begins with mentioning various datasets used for the experiments in 5.1, followed by the experiment settings in 5.2, and data pre-processing procedures in 5.3. Subsequently, the results of the ablation studies on different model variables are presented, along with an evaluation of the FDMSE-ISL dataset (referred to as the working dataset), and an assessment of the proposed HWGAT model across multiple isolated ISL datasets, as discussed in Section 5.4.

5.1. Datasets

The datasets FDMSE-ISL, INCLUDE [44], AUTSL [43], LSA64 [39], WLASL [22] are tested with 5 different models. The details of the datasets are described in Section 2. A detailed description of the FDMSE-ISL dataset is presented in Section 3. A comparison (with respect to the number of signs, number of videos, number of unique signers, video source, and total duration) of all these datasets is shown in Table 1.

For all our evaluations, we strictly adhere to the data partitions provided by the respective datasets. Since there was no validation set available in the INCLUDE dataset, we partitioned out 10% of the train set to form the validation set.

For the extensive ablation studies, we consider a 20% subset of the FDMSE-ISL dataset. We call this subset FDMSE-ISL400. It contains 400 classes with 8000 video samples. These 400 classes were chosen from 2002 classes with Simple Random Sampling without replacement (SR-SWOR) sampling procedure to preserve the frame statistics.

5.2. Experimental Settings

The performance of the keypoint-based approaches depend on the effective detection of the body keypoints. We use MediaPipe holistic [26] for pose estimation due to its performance balance in pose estimation accuracy and processing speed when compared to other methods [7, 28, 50]. The MediaPipe holistic gives a total of 543, keypoints in 3D (468 for face, 33 for pose, and 21 per hand) per video frame. Out of these, we pick 27 keypoints of interest (3 facial (nose, 2 eyes), 2 shoulders, 2 elbows, and 10 keypoints from each hand) to construct the spatial graph.

We implemented all the models using the PyTorch toolbox³ and trained on a system with Xeon® Gold 32 Core Processor, NVIDIA A100 80G GPU, and running Ubuntu 22.04. To train the models AdamW Optimizer was used with an initial learning rate of $1e^{-4}$ with the Cosine Annealing scheduler having a patience of 20 epochs. The max training epoch was set to 4000 with early stopping on validation loss and patience of 400 epochs. The objective function used for training is label smoothed cross entropy loss [12]. For all our experiments, we report top-1 and top-5 per instance accuracy as the performance measure.

5.3. Data Pre-processing and Augmentations

Several data pre-processing techniques were used to normalize the data. MediaPipe holistic generates keypoints in 3D with each ordinate in [0,1]. In our settings, [0,0] and [1,1] correspond to the top left and bottom right corner of the video frame. We convert all the keypoints to video frame coordinates using the frame size. In real-life video recording scenarios, actors can appear anywhere within the image plane with varying scales depending on the camera position. We normalise the keypoint coordinates to achieve location and scale invariance for keypoints using dynamic bounding boxes. Additionally, we apply shear and rotation transformations to the keypoints during training to introduce subtle random variations, inspired by Selvaraj *et al.* [42].

MediaPipe holistic sometimes fails to detect all the keypoints. We approximate these missing keypoints using spherical linear interpolation technique. To introduce the variability of the missing keypoints, we further introduce some random masking on detected keypoints and use similar interpolation to approximate those keypoints. This technique of replacing masked values ensures a stable learning process for the model.

According to the ISL experts, signing speed differs from signer to signer. To incorporate speed variability, we introduce the temporal augmentation technique by randomly decreasing or increasing the number of frames through Simple Random Sampling Without Replacement (SRSWOR) or Simple Random Sampling with replacement (SRSWR) sampling procedure respectively. In order to equalize the length of the video clips shorter than that of the model requirement, we perform temporal augmentation by padding random offsets at the beginning and end suitably. Conversely, videos of longer length are downsized to the model requirement through a uniform sampling of the frames. These augmentation techniques were found to increase the model robustness during training.

³<https://pytorch.org/>

Table 3. Impact of the number of spatial windows on FDMSE-ISL400 dataset.

# Spatial windows ⁴	Test Accuracy	
	Top-1	Top-5
1	95.37	99.22
4	95.94	99.44

Table 4. Impact of temporal block size on FDMSE-ISL400 dataset.

Temporal block size	Test Accuracy	
	Top-1	Top-5
2	95.94	99.44
4	94.97	99.31

Table 5. Impact of temporal shift on FDMSE-ISL400 dataset.

Shifting window	Test Accuracy	
	Top-1	Top-5
Without Shift	94.97	99.31
With Shift	95.94	99.44

Table 6. Impact of edge bias on FDMSE-ISL400 dataset.

Edge bias type	Test Accuracy	
	Top-1	Top-5
Learnable Edge Bias	95.53	99.41
Without Edge Bias	95.16	99.00
With Edge Bias	95.94	99.44

Table 7. Impact of regularizer on FDMSE-ISL400 dataset.

Presence of regularizer	Test Accuracy	
	Top-1	Top-5
No Regularizer	95.94	99.44
Regularizer	96.63	99.47

Table 8. Sample test results of HWGAT on FDMSE-ISL where the model fails to correctly recognize classes due to inter-class similarity. The digit in parenthesis indicate the number of occurrences of the sign in the test dataset.

Ground Truth	Predicted Output
Eye(8)	Sour(1), Eye(1), Nose(5), Think(1)
0/Zero(6)	O(4), Ear(1), 0/Zero(1)
These(8)	These(1), Those(7)
Seat(8)	Bench(5), Seat(3)
Low(8)	Low(4), Decrease(1), Short/Young(3)

5.4. Results

5.4.1 Ablation Study

The ablation study was performed on different variables, such as *number of spatial windows*, *temporal blocks size*, *temporal shift*, *edge bias* and *regularizer*, of the proposed HWGAT model using the FDMSE-ISL400 dataset. We report top-1 and top-5 per instance accuracy as the performance measures.

Number of spatial windows: The division of each spatial graph into spatial windows is a distinct feature of the input representation. Based on subdividing we have experimented with two cases, namely, with no subdivisions which we call the 1-spatial window case, and the other as depicted in Fig. 4 which we call the 4-spatial window case.

The results of the two windowing cases are shown in Table 3. We see that the 4-spatial window case gives better performance of top-1 95.94% and top-5 99.44% accuracy compared to the 1-spatial window case.

Temporal block size: The accuracy is the highest when the temporal block size is set to 2 as shown in Table 4. The temporal block size being 2 enables the model to capture the motion in consecutive frames.

Effect of temporal shift: Table 5 shows the results of the temporal shift mechanism as described in Section 4.2.1. The temporal shifting allows the information propagation between consecutive temporal blocks resulting in better top-1 and top-5 accuracies compared to the case of no shifting.

Effect of edge bias: The proposed edge bias described in Section 4.2.1 yields improved results by a slight margin as shown in Table 6. Compared to the model without edge bias, the proposed edge bias-based model improves accuracy by 0.78 and 0.44 percentage points in top-1 and top-5, respectively. Furthermore, this edge bias-based model demonstrates slightly better performance than the model with learnable edge bias. We believe this improvement is mainly due to the attention mechanism being restricted to each spatio-temporal block.

Impact of regularizer: The proposed attention dropout regularization technique described in Section 4.2.1 gives slightly improved performance (0.69 percentage point in top-1 and 0.03 percentage point in top-5) compared to the model without regularize.

5.4.2 Evaluation of proposed dataset

The FDMSE-ISL and INCLUDE [44] datasets are tested with the proposed model HWGAT and three other models of which one is a baseline transformer-based model and the other two are state-of-the-art keypoint-based models ST-GCN [16] and SL-GCN [16]. The results of the experiments are shown in Table 10. All the models perform relatively poorly on the FDMSE-ISL dataset compared to IN-

Table 9. Sample test results of the HWGAT model on the FDMSE-ISL dataset indicating that the model confuses certain composite classes with their corresponding atomic signs. The digit in parenthesis indicate the number of occurrences of the sign in the test dataset.

Ground Truth	Atomic Signs	Predicted Output
Delhi(8)	D, D	D(2), Delhi(6)
Inaugurate(8)	Scissors, Open	Inaugurate(7), Open(1)
Lecturer(8)	L, Teacher	Lecturer(7), Teacher(1)
Mosque(8)	Muslim, Pray	Muslim(1), Mosque(7)
False/Negative(8)	Meaning, Wrong	Wrong(1), False/Negative(7)

Table 10. Comparison of results (accuracy) obtained by employing various models on the two ISL datasets: INCLUDE and FDMSE-ISL.

Model	INCLUDE		FDMSE-ISL	
	Top-1	Top-5	Top-1	Top-5
Transformer	94.85	99.14	89.71	97.95
ST-GCN [16]	96.69	99.14	93.57	99.01
SL-GCN [16]	96.57	99.26	93.39	98.98
HWGAT	97.67	99.26	93.86	99.19
HWGAT (Finetuned)	97.79	99.26	-	-

Table 11. Comparison of results (accuracy) obtained by employing various models on the Argentinian, Turkish and American SL datasets.

Model	LSA64		AUTSL		WLASL	
	Top-1	Top-5	Top-1	Top-5	Top-1	Top-5
Pose-GRU [22]	-	-	-	-	22.54	49.81
Pose-TGCN [22]	-	-	-	-	23.65	51.75
Transformer	90.00	98.12	90.19	98.61	23.20	-
ST-GCN [16]	92.81	98.43	90.67	98.66	34.40	66.57
SL-GCN [16]	98.13	100.00	95.02	-	41.65	74.68
HWGAT	97.81	99.84	95.43	99.17	43.28	74.92
HWGAT (Finetuned)	98.59	99.84	95.80	99.49	48.49	80.86

CLUDE [44]. Such poor performance on FDMSE-ISL can be attributed to, but is not limited to, the following three factors:

1. A higher number of classes is a contributing factor. We obtained an accuracy of 96.63% on the FDMSE-ISL400 subset having 400 classes (shown in Table 7), while the same study on the entire FDMSE-ISL (working dataset) having 2002 classes yielded an accuracy of only 93.86% (Table 10).
2. The co-occurrence of independent atomic signs within composite signs creates confusion for the model, leading to misclassification between the composite sign and its atomic sign subset, as shown in Table 9. For example, the sign word *Lecturer* is a composition of two atomic signs: *L* and *Teacher* but the model predicts it as either *Lecturer* or *Teacher*.
3. There is a significant inter-class similarity between certain distinct signs, such as *Low* vs. *Short/Young* and *Seat* vs. *Bench*, as depicted in Fig. 9. Additional examples of such similarities are tabulated in Table 8.

Thus FDMSE-ISL is a more challenging dataset for ISL recognition.

To observe the effect of knowledge transfer, we pre-trained the proposed model on FDMSE-ISL and fine-tuned it on the INCLUDE dataset. We achieved top-1 with 97.79% and top-5 with 99.26% as shown in the last row of Table 10. This result shows the utility of FDMSE-ISL for the ISL recognition task as a pre-trained dataset on a relatively smaller isolated ISL datasets similar to the INCLUDE dataset.

5.4.3 Evaluation of proposed model

The proposed HWGAT model outperforms or shows comparable results to other models on both the FDMSE-ISL and INCLUDE datasets, as demonstrated in Table 10. Additionally, Table 11 reveals that HWGAT consistently achieves superior performance on three additional candidate SL datasets. Specifically, it attains the highest top-1 (95.43%, 43.28%) and top-5 (99.17%, 74.92%) accuracies for the AUTSL [43] and WLASL [22] datasets, respectively.



Figure 9. Two examples depicting similarity of signs for two different classes. In (a), we note that the signs of *Low* and *Short/Young* are visually similar and likewise in (b) for *Seat* and *Bench*.

Even for the LSA64 [39] dataset, the proposed model exhibits comparable performance in terms of both top-1 and top-5 accuracy measures.

Furthermore, The model is found to achieve the highest top-1 performance for all the datasets as shown in the last row of Table 11 when it was pre-trained on the FDMSE-ISL dataset. Thus, the FDMSE-ISL dataset can be used for pre-training a model to potentially improve the model’s performance on other SL datasets.

6. Conclusion

In this paper, we introduce FDMSE-ISL, a novel large-scale isolated Indian Sign Language dataset, and propose a Hierarchical Windowed Graph Attention Network (HWGAT) model for sign language recognition.

The FDMSE-ISL dataset is unique for its extensive size, gender balance, class balance, multi-modality, and multi-view perspectives. The HWGAT model leverages the human upper body keypoint graph to capture distinct sign characteristics by focusing attention on interacting body parts.

Our empirical results demonstrate the significance of the dataset and the effectiveness of the HWGAT model. Specifically, a comparative analysis of FDMSE-ISL with the well-known isolated ISL dataset, INCLUDE, using various state-of-the-art keypoint-based models, highlights the comprehensiveness and complexity of the presented dataset. The HWGAT model was evaluated on diverse sign language datasets, including Indian, American, Argentinian, and Turkish. The HWGAT model consistently outperformed or performed comparably to existing state-of-the-art keypoint-based models. Furthermore, when pre-trained on FDMSE-ISL and subsequently fine-tuned on these diverse datasets, HWGAT exhibited superior recognition accuracy, emphasising the importance of the dataset.

The FDMSE-ISL dataset’s rich diversity can accelerate research in ISL recognition and be beneficial for other sign language tasks. Its multi-view and data type inclusion can aid in keypoint correction, pose estimation, 3D model creation, and general gesture recognition. Additionally, our

word grouping method based on glosses can support teaching and learning Indian Sign Language in educational settings.

Acknowledgement

This work is partially funded by VECC, Kolkata. We thank Mr. Subhankar Nag for the data processing and model discussions.

References

- [1] Nikolas Adaloglou, Theodoris Chatzis, Ilias Papastratis, Andreas Stergioulas, Georgios Th Papadopoulos, Vassia Zacharopoulou, George J Xydopoulos, Klimnis Atzakis, Dimitris Papazachariou, and Petros Daras. A comprehensive study on deep learning-based methods for sign language recognition. *IEEE Transactions on Multimedia*, 24:1750–1762, 2021. 1, 3
- [2] S Ajay, Ajith Potluri, Sara Mohan George, R Gaurav, and S Anusri. Indian sign language recognition using random forest classifier. In *2021 IEEE International Conference on Electronics, Computing and Communication Technologies (CONECCT)*, pages 1–6, 2021. 3
- [3] Samuel Albanie, Gül Varol, Liliane Momeni, Hannah Bull, Triantafyllos Afouras, Himel Chowdhury, Neil Fox, Bencie Woll, Rob Cooper, Andrew McParland, et al. Bbc-oxford british sign language dataset. *arXiv preprint arXiv:2111.03635*, 2021. 2
- [4] Vassilis Athitsos, Carol Neidle, Stan Sclaroff, Joan Nash, Alexandra Stefan, Quan Yuan, and Ashwin Thangali. The american sign language lexicon video dataset. In *Conference on Computer Vision and Pattern Recognition Workshops (CVPR)*, pages 1–8, 2008. 2, 3
- [5] Matyáš Boháček and Marek Hruš. Sign pose-based transformer for word-level sign language recognition. In *Proceedings of the IEEE/CVF winter conference on applications of computer vision (WACV)*, pages 182–191, 2022. 4
- [6] Necati Cihan Camgoz, Oscar Koller, Simon Hadfield, and Richard Bowden. Sign language transformers: Joint end-to-end sign language recognition and translation. In *Proceedings of the IEEE/CVF Conference on Computer Vision and Pattern Recognition (CVPR)*, 2020. 4

- [7] Zhe Cao, Tomas Simon, Shih-En Wei, and Yaser Sheikh. Realtime multi-person 2d pose estimation using part affinity fields. In *Proceedings of the IEEE/CVF Conference on Computer Vision and Pattern Recognition (CVPR)*, pages 7291–7299, 2017. 4, 10
- [8] Navneet Dalal and Bill Triggs. Histograms of oriented gradients for human detection. In *Proceedings of the IEEE/CVF Conference on Computer Vision and Pattern Recognition (CVPR)*, volume 1, pages 886–893, 2005. 3
- [9] Soumen Das, Saroj Kr. Biswas, and Biswajit Purkayastha. Occlusion robust sign language recognition system for indian sign language using cnn and pose features. *Multimedia Tools and Applications*, 2024. 3
- [10] Deafness and hearing loss. <https://www.who.int/news-room/fact-sheets/detail/deafness-and-hearing-loss>. Accessed: 2024-04-10. 1
- [11] Sarah Ebling, Necati Cihan Camgöz, Penny Boyes Braem, Katja Tissi, Sandra Sidler-Miserez, Stephanie Stoll, Simon Hadfield, Tobias Haug, Richard Bowden, Sandrine Tornay, et al. Smile swiss german sign language dataset. In *Proceedings of the 11th International Conference on Language Resources and Evaluation (LREC)*, 2018. 3
- [12] Tong He, Zhi Zhang, Hang Zhang, Zhongyue Zhang, Junyuan Xie, and Mu Li. Bag of tricks for image classification with convolutional neural networks. In *Proceedings of the IEEE/CVF Conference on Computer Vision and Pattern Recognition (CVPR)*, pages 558–567, 2019. 10
- [13] Berthold KP Horn and Brian G Schunck. Determining optical flow. *Artificial Intelligence*, 17(1-3):185–203, 1981. 3
- [14] Jie Huang, Wengang Zhou, Qilin Zhang, Houqiang Li, and Weiping Li. Video-based sign language recognition without temporal segmentation. In *Proceedings of the AAAI Conference on Artificial Intelligence (AAAI)*, volume 32, 2018. 3
- [15] Indian sign language dictionary. <https://indiansignlanguage.org/>. Accessed: 2024-04-10. 4
- [16] Songyao Jiang, Bin Sun, Lichen Wang, Yue Bai, Kunpeng Li, and Yun Fu. Skeleton aware multi-modal sign language recognition. In *Proceedings of the IEEE/CVF Conference on Computer Vision and Pattern Recognition (CVPR)*, pages 3413–3423, 2021. 3, 4, 6, 11, 12
- [17] Abhinav Joshi, Ashwani Bhat, Pradeep S, Priya Gole, Shashwat Gupta, Shreyansh Agarwal, and Ashutosh Modi. CISLR: Corpus for Indian Sign Language recognition. In *Proceedings of the 2022 Conference on Empirical Methods in Natural Language Processing (EMNLP)*, pages 10357–10366, 2022. 2, 3
- [18] G. Khartheesvar, Mohit Kumar, Arun Kumar Yadav, and Divakar Yadav. Automatic indian sign language recognition using mediapipe holistic and lstm network. *Multimedia Tools and Applications*, 2023. 4
- [19] P.V.V. Kishore and Panakala rajesh kumar. A video based indian sign language recognition system (inslr) using wavelet transform and fuzzy logic. *International Journal of Engineering and Technology*, 4:537–542, 01 2012. 2
- [20] Oscar Koller, Hermann Ney, and Richard Bowden. Deep hand: How to train a cnn on 1 million hand images when your data is continuous and weakly labelled. In *Proceedings of the IEEE/CVF Conference on Computer Vision and Pattern Recognition (CVPR)*, pages 3793–3802, 2016. 3
- [21] Oscar Koller, O Zargaran, Hermann Ney, and Richard Bowden. Deep sign: Hybrid cnn-hmm for continuous sign language recognition. In *Proceedings of the British Machine Vision Conference (BMVC)*, 2016. 3
- [22] Dongxu Li, Cristian Rodriguez, Xin Yu, and Hongdong Li. Word-level deep sign language recognition from video: A new large-scale dataset and methods comparison. In *Proceedings of the IEEE/CVF Conference on Computer Vision and Pattern Recognition (CVPR)*, pages 1459–1469, 2020. 1, 2, 3, 4, 10, 12
- [23] Tao Liu, Wengang Zhou, and Houqiang Li. Sign language recognition with long short-term memory. In *2016 IEEE International Conference on Image Processing (ICIP)*, pages 2871–2875, 2016. 1, 3, 4
- [24] Ze Liu, Yutong Lin, Yue Cao, Han Hu, Yixuan Wei, Zheng Zhang, Stephen Lin, and Baining Guo. Swin transformer: Hierarchical vision transformer using shifted windows. In *2021 IEEE/CVF International Conference on Computer Vision (ICCV)*, pages 9992–10002, 2021. 8
- [25] David G Lowe. Distinctive image features from scale-invariant keypoints. *International Journal of Computer Vision*, 60:91–110, 2004. 3
- [26] Camillo Lugaresi, Jiuqiang Tang, Hadon Nash, Chris McClanahan, Esha Uboweja, Michael Hays, Fan Zhang, Chuo-Ling Chang, Ming Guang Yong, Juhyun Lee, et al. Mediapipe: A framework for building perception pipelines. *arXiv preprint arXiv:1906.08172*, 2019. 4, 10
- [27] Debapriya Maji, Soyeb Nagori, Manu Mathew, and Deepak Poddar. Yolo-pose: Enhancing yolo for multi person pose estimation using object keypoint similarity loss. In *Proceedings of the IEEE/CVF Conference on Computer Vision and Pattern Recognition (CVPR)*, pages 2637–2646, 2022. 4
- [28] Openmmlab pose estimation toolbox and benchmark. <https://github.com/open-mmlab/mmpose>. Accessed: 2024-04-10. 4, 10
- [29] Liliane Momeni, Gul Varol, Samuel Albanie, Triantafyllos Afouras, and Andrew Zisserman. Watch, read and lookup: Learning to spot signs from multiple supervisors. In *Proceedings of the Asian Conference on Computer Vision (ACCV)*, 2020. 2, 3
- [30] Anup Nandy, Jay Shankar Prasad, Soumik Mondal, Pavan Chakraborty, and G. C. Nandi. Recognition of isolated indian sign language gesture in real time. In *Information Processing and Management*, pages 102–107, 2010. 2
- [31] Oğulcan Özdemir, Ahmet Alp Kindiroğlu, Necati Cihan Camgöz, and Lale Akarun. Bosphorussign22k sign language recognition dataset. In *Proceedings of the LREC2020 9th Workshop on the Representation and Processing of Sign Languages: Sign Language Resources in the Service of the Language Community, Technological Challenges and Application Perspectives*, pages 181–188, 2020. 3
- [32] Ronald Poppe. A survey on vision-based human action recognition. *Image and Vision Computing*, 28(6):976–990, 2010. 2

- [33] Lawrence Rabiner and Biinghwang Juang. An introduction to hidden markov models. *IEEE ASSP Magazine*, 3(1):4–16, 1986. [3](#)
- [34] Umer Rafi, Bastian Leibe, Juergen Gall, and Ilya Kostrikov. An efficient convolutional network for human pose estimation. In *Proceedings of the British Machine Vision Conference (BMVC)*, volume 1, page 2, 2016. [4](#)
- [35] JL Raheja, Anand Mishra, and Ankit Chaudhary. Indian sign language recognition using svm. *Pattern Recognition and Image Analysis*, 26:434–441, 2016. [3](#)
- [36] G Anantha Rao, K Syamala, PVV Kishore, and ASCS Sasstry. Deep convolutional neural networks for sign language recognition. In *2018 Conference on Signal Processing and Communication Engineering Systems (SPACES)*, pages 194–197. IEEE, 2018. [3](#)
- [37] J. Rekha, J. Bhattacharya, and S. Majumder. Shape, texture and local movement hand gesture features for indian sign language recognition. In *3rd International Conference on Trendz in Information Sciences & Computing (TISC)*, pages 30–35, 2011. [2](#)
- [38] Pengfei Ren, Haifeng Sun, Qi Qi, Jingyu Wang, and Weiting Huang. Srn: Stacked regression network for real-time 3d hand pose estimation. In *Proceedings of the British Machine Vision Conference (BMVC)*, page 112, 2019. [4](#)
- [39] Franco Ronchetti, Facundo Quiroga, Cesar Estrebow, Laura Lanzarini, and Alejandro Rosete. Lsa64: A dataset of argentinian sign language. *XX II Congreso Argentino de Ciencias de la Computación (CACIC)*, 2016. [1](#), [2](#), [3](#), [10](#), [13](#)
- [40] Wendy Sandler and Diane Carolyn Lillo-Martin. *Sign language and linguistic universals*. Cambridge University Press, Cambridge, United Kingdom, 2006. [1](#)
- [41] Zed Sevcikova Sehyr, Naomi Caselli, Ariel M Cohen-Goldberg, and Karen Emmorey. The asl-lex 2.0 project: A database of lexical and phonological properties for 2,723 signs in american sign language. *The Journal of Deaf Studies and Deaf Education*, 26(2):263–277, 2021. [3](#)
- [42] Prem Selvaraj, Gokul Nc, Pratyush Kumar, and Mitesh M Khapra. Openhands: Making sign language recognition accessible with pose-based pretrained models across languages. In *Proceedings of the 60th Annual Meeting of the Association for Computational Linguistics (Volume 1: Long Papers)*, pages 2114–2133, 2022. [4](#), [6](#), [10](#)
- [43] Ozge Mercanoglu Sincan and Hacer Yalim Keles. Autsl: A large scale multi-modal turkish sign language dataset and baseline methods. *IEEE Access*, pages 181340–181355, 2020. [1](#), [2](#), [3](#), [10](#), [12](#)
- [44] Advait Sridhar, Rohith Gandhi Ganesan, Pratyush Kumar, and Mitesh Khapra. Include: A large scale dataset for indian sign language recognition. In *Proceedings of the 28th ACM International Conference on Multimedia (ACMMM)*, pages 1366–1375, 2020. [1](#), [2](#), [3](#), [5](#), [10](#), [11](#), [12](#)
- [45] Matthew Tancik, Pratul P. Srinivasan, Ben Mildenhall, Sara Fridovich-Keil, Nithin Raghavan, Utkarsh Singhal, Ravi Ramamoorthi, Jonathan T. Barron, and Ren Ng. Fourier features let networks learn high frequency functions in low dimensional domains. In *Advances in Neural Information Processing Systems (NeurIPS)*, 2020. [8](#)
- [46] Alaa Tharwat, Tarek Gaber, Aboul Ella Hassanien, Mohamed K Shahin, and Basma Refaat. Sift-based arabic sign language recognition system. In *Afro-European Conference for Industrial Advancement: Proceedings of the First International Afro-European Conference for Industrial Advancement (AECIA) 2014*, pages 359–370, 2015. [1](#), [3](#)
- [47] Hamid Vaezi Joze and Oscar Koller. Ms-asl: A large-scale data set and benchmark for understanding american sign language. In *The British Machine Vision Conference (BMVC)*, September 2019. [2](#), [3](#)
- [48] Ashish Vaswani, Noam Shazeer, Niki Parmar, Jakob Uszkoreit, Llion Jones, Aidan N Gomez, L ukasz Kaiser, and Illia Polosukhin. Attention is all you need. In *Advances in Neural Information Processing Systems (NeurIPS)*, 2017. [2](#), [8](#), [9](#)
- [49] Hanjie Wang, Xiujuan Chai, Xiaopeng Hong, Guoying Zhao, and Xilin Chen. Isolated sign language recognition with grassmann covariance matrices. *ACM Transactions on Accessible Computing (TACCESS)*, 8(4):1–21, 2016. [3](#)
- [50] Jingdong Wang, Ke Sun, Tianheng Cheng, Borui Jiang, Chaorui Deng, Yang Zhao, Dong Liu, Yadong Mu, Mingkui Tan, Xinggang Wang, et al. Deep high-resolution representation learning for visual recognition. *IEEE Transactions on Pattern Analysis and Machine Intelligence*, 43(10):3349–3364, 2020. [4](#), [10](#)
- [51] Sijie Yan, Yuanjun Xiong, and Dahua Lin. Spatial temporal graph convolutional networks for skeleton-based action recognition. In *Proceedings of the AAAI conference on artificial intelligence (AAAI)*, volume 32, 2018. [4](#), [6](#)
- [52] Lin Zehui, Pengfei Liu, Luyao Huang, Junkun Chen, Xipeng Qiu, and Xuanjing Huang. Dropattention: A regularization method for fully-connected self-attention networks. *arXiv preprint arXiv:1907.11065*, 2019. [9](#)
- [53] Jihai Zhang, Wengang Zhou, Chao Xie, Junfu Pu, and Houqiang Li. Chinese sign language recognition with adaptive hmm. In *2016 IEEE International Conference on Multimedia and Expo (ICME)*, pages 1–6, 2016. [1](#), [2](#), [3](#)
- [54] Zhiming Zou, Kenkun Liu, Le Wang 0003, and Wei Tang. High-order graph convolutional networks for 3d human pose estimation. In *Proceedings of the British Machine Vision Conference (BMVC)*, 2020. [4](#)
- [55] Ronglai Zuo, Fangyun Wei, and Brian Mak. Natural language-assisted sign language recognition. In *Proceedings of the IEEE/CVF Conference on Computer Vision and Pattern Recognition*, pages 14890–14900, 2023. [3](#)